ELSEVIER

Journal of Fluids and Structures 20 (2005) 451–464

JOURNAL OF FLUIDS AND STRUCTURES

www.elsevier.nl/locate/jnlabr/yjfls

Vortex-shedding characteristics in the wake of an oscillating airfoil at low Reynolds number

Y.W. Jung[a], S.O. Park[b,*]

[a]*Department of Aeropropulsion, Korea Aerospace Research Institute, 45 Eoeun-Dong, Yuseong-Gu, Daejeon 305-333, Republic of Korea*
[b]*Department of Aerospace Engineering, Korea Advanced Institute of Science and Technology, 373-1 Kuseong-Dong, Yuseong-Gu, Daejeon 305-701, Republic of Korea*

Received 6 August 2003; accepted 9 November 2004

Abstract

An experimental investigation was carried out to study the unsteady characteristics of vortex shedding in the near wake of an oscillating airfoil. The airfoil was given a harmonic pitching motion about the quarter-chord axis at four reduced frequencies: 0.1, 0.2, 0.3, and 0.4. The mean incidence and the oscillating amplitude were 0° and 3°, respectively. The velocity in the wake was measured by hot-wire anemometry. Smoke-wire visualization was also carried out to look into the link between the boundary layer flow and the shedding frequency variation. To analyze the frequency characteristics of the vortex shedding, we composed a short-time spectrum by the autoregressive (AR) method and a moving window. It was found that the shedding frequency in the wake of oscillating airfoil was much different from that for the case of steady airfoil at a given angle of attack, implying that the state of the boundary layer dictated the vortex-shedding characteristics. The vortex-shedding frequency was found to vary with the phase angle of oscillation, not with the angle of attack, for a given reduced frequency. The range of variation of the shedding frequency was diminished as the reduced frequency of oscillation increased.

1. Introduction

The characteristics of airfoil aerodynamics at low Reynolds numbers have become of interest in conjunction with the emergence of micro air and underwater vehicles. Often, the motion of such vehicles experiences an unsteady condition, such as flapping and pitching. According to boundary layer studies, the flow field at low Reynolds numbers, typically ranging from 10^4 to 10^5 based on the chord length, involves transition from laminar to turbulent flow. Especially, at a Reynolds number below 5×10^4, it is unusual for reattachment to occur on the airfoil surface (Lissaman, 1983; Hsiao et al., 1989). In this range, when the angle of attack is small, discrete vortices are formed and shed into the wake region. Several investigators studied the vortex-shedding characteristics of airfoils. Stuber and Gharib (1990) perturbed the airfoil boundary layers through the use of the strip heater technique and examined the nonlinear interaction of multiple frequencies in the wake of an airfoil. Huang and Lin (1995) identified several characteristic modes of the oscillating unsteady flow at low angle of attack and Reynolds number. They showed that the characteristic modes were closely related to the boundary layer behavior on the airfoil surfaces. Koochesfahani (1989) studied experimentally the vortical

*Corresponding author. Tel.: +82 42 869 3713; fax: +82 42 869 3710.
E-mail address: sopark@kaist.ac.kr (S.O. Park).

0889-9746/$ - see front matter © 2004 Elsevier Ltd. All rights reserved.
doi:10.1016/j.jfluidstructs.2004.11.002

flow patterns in the wake of an airfoil pitching at small amplitudes and showed that at certain high reduced frequencies the wake transforms into a jet-like flow with thrust generation. Triantafyllou et al. (1991) found that optimal foil efficiency, which is the ratio of thrust to input power, is achieved when the Strouhal number, based on the airfoil oscillating frequency and the maximum excursion of the airfoil trailing edge, was between 0.25 and 0.35. They focused on the vortex-shedding behind an oscillating airfoil at high reduced frequencies in relation to the thrust generation and the lock-on phenomenon. Recently, Chang and Eun (2003) reported mean velocity and turbulent intensity profiles in the near wake of an elliptic airfoil oscillating in pitch at the Reynolds number of 3.3×10^4.

So far, little attention has been given to the study of the vortex-shedding at low reduced frequencies. A primary purpose of the present work is to find out how the shedding frequency changes with the oscillatory motion of the airfoil at low reduced frequencies. The oscillatory nature of the boundary layer flow over an oscillating airfoil is also examined since the vortex in the near wake is influenced directly by the boundary layer and vice versa. The smoke-wire technique and hot-wire anemometry are employed for the flow visualization and the velocity measurement, respectively. The frequency characteristics of the unsteady wake behind an oscillating airfoil have to be deduced based on very short data segments. The time-varying frequency characteristic is then tracked by examining the variations in spectral estimates from segment to segment. For the spectral estimation of each segment, a short-time autoregressive (AR) method is adopted. When only a small number of samples is available because of the unsteady nature of the flow, the AR method is more useful and reliable than the Fast Fourier transform (FFT) method for spectral analysis, since its resolution is higher than that of the FFT method (Kay, 1982; Marple, 1987).

2. Experimental apparatus

The experiment was performed in a small open-circuit wind tunnel of $20 \times 30\,\text{cm}^2$ test-section having the length of 120 cm. The free-stream turbulence intensity in the test-section was within 0.15% and the maximum velocity was approximately 15 m/s. An airfoil of NACA 0012 profile was mounted horizontally into the test-section. The chord length and the span of the airfoil were 10 and 19.8 cm, respectively. The gap between the airfoil and the sidewall was 0.1 cm. A schematic of the experimental set-up is given in Fig. 1. The airfoil was made of aluminum alloy and the airfoil surface was anodized to reduce the roughness and prevent corrosion. Pitching oscillation about the quarter-chord axis was provided by a crank-connecting rod mechanism, driven by a variable-speed ac motor. The instantaneous angle of attack α can be expressed as $\alpha = \alpha_0 + \alpha_1 \sin \omega t$. Throughout the present experiment, the mean incidence α_0 and the oscillating amplitude α_1 were set to be 0° and 3°, respectively. The airfoil is in pitch-up stroke when $0^\circ \leqslant \omega t \leqslant 90^\circ$ and $270^\circ \leqslant \omega t \leqslant 360^\circ$, and is in pitch-down stroke when $90^\circ \leqslant \omega t \leqslant 270^\circ$. Four values of the reduced frequency κ, defined as $\kappa = \omega c/2U_\infty$, were considered: $\kappa = 0.1$, 0.2, 0.3, and 0.4. Here, ω is the circular frequency of the airfoil oscillation, c is the chord length, and U_∞ is the free-stream velocity. The free-stream velocity was set at 4 m/s and the corresponding Reynolds number, based on the chord length, was 27 000. As the aspect ratio of the airfoil in the present experiment is only 1.98, the two-dimensionality of the flow can be doubtful. However, Carr et al. (1977) investigated the problem of two-dimensionality in their experiment with a wing having an aspect ratio of 1.62, and observed that the wing–wall

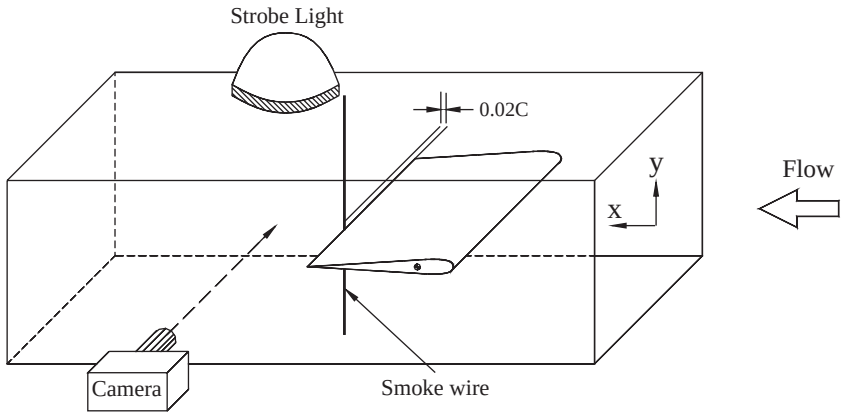

Fig. 1. Schematic of experimental set-up.

interaction had negligible effects when $\kappa \geqslant 0.10$, contrary to the static-airfoil test. In the preliminary phase of the present work, we observed that the streaklines coming out from the smoke-wire placed spanwise just above the airfoil surface at about the quarter chord were not distorted for most of the wing surface, except for the wing-tip regions close to the tunnel wall. We thus believe that the present set-up is not likely to entail any significant three-dimensional effects.

A constant-temperature hot-wire anemometer (AN-1003) and a four X-wire probe array were employed for the velocity measurements. With this four X-wire probe array, we measured the velocity signal at four transverse locations simultaneously at a given downstream station. The distance between two adjacent X-wire probes was 4 mm. The hot-wire probe was mounted on a support in the center plane of the test-section. A computer-controlled 2-D traversing mechanism moved the probe support to the measuring station and the spatial resolution of the traverse was 0.01 mm.

Flow visualization was carried out using the smoke-wire technique. To visualize streaklines, an electrically resistive nichrome wire of 0.1 mm diameter was installed vertically at the location of $0.02c$ downstream from the trailing edge. The smoke streaklines, lighted by a stroboscope with 16–32 μs flash duration, trace the unsteady pattern of reverse flow and the evolution of vortex-shedding. Photographs were taken with a 35 mm Nikon SLR camera equipped with a standard lens ($f = 1.4$) using ASA 400 film. A close-up lens is used to take a better photograph of the trailing edge region. The stroboscope was capable of external triggering, making it possible to take a picture at a given phase with the open-flash technique, in which the photograph is taken under the stroboscope light when the iris of camera lens is open.

3. Data acquisition and reduction

3.1. Data acquisition

A reference trigger signal to initiate data sampling for ensemble averaging was generated by a LED and photo-TR circuit attached to the driving disk of the crank-connecting-rod mechanism. The system was adjusted to produce one trigger pulse per revolution when the airfoil was at a desired incidence. This system was also used to trigger the stroboscope for the smoke-wire visualization.

As mentioned earlier, four values of the reduced frequency κ were considered: $\kappa = 0.1$, 0.2, 0.3, and 0.4. For the case of $\kappa = 0.1$, the velocity signal was sampled at 3 kHz and the cut-off frequency of an anti-aliasing filter was set at 1 kHz. For the other cases, the sampling frequency was 10 kHz and the cut-off frequency of an anti-aliasing filter was 3 kHz. Since the shedding frequencies are less than 200 Hz, the sampling frequency of 3 kHz is sufficient to produce the time series of the wake velocity signal. As the reduced frequency becomes larger at a fixed velocity, the period of airfoil oscillation becomes smaller. Consequently, the number of data samples per period of oscillation decreases. It is therefore necessary to increase the sampling rate to have a sufficiently large size of data for the spectral analysis; this will be explained later in more detail. For the cases of $\kappa = 0.2$, 0.3 and 0.4, the sampling frequency of 10 kHz is selected. For each measurement, the velocity signal was taken over a time period a little longer than one period of the airfoil oscillation. For example, for the case of $\kappa = 0.2$, the period of oscillation is about 0.4 s. The data were taken for 0.5 s, yielding 5000 samples. The measurement was repeated 250 times for the ensemble average.

In the steady case, we measured the velocity at various downstream stations in the near wake from $0.01c$ to $1.0c$. Especially, in the region from the trailing edge to $0.15c$ downstream station, the probe was traversed with an interval of $0.01c$ to determine the measuring station. For the case of $\alpha = 0^\circ$, we found that the velocity signal was influenced by the reverse flow, up to $x/c = 0.08$. For this reason, we used the velocity signal measured at downstream stations beyond $0.1c$. In the unsteady case, by a similar argument, we used the signal measured at $x/c = 0.1$ and 0.3 for spectral analysis.

The velocities at four transverse stations at a given downstream station were measured simultaneously by a four X-wire probe array, with a vertical spacing of 4 mm. Let us designate the four X-wires as W1, W2, W3 and W4, starting from the bottom. The wires W2 and W3 were used as the main probes for velocity profile measurement. W1 and W4 were used as detectors to judge the flow state of the wake. The cross-correlation coefficient of the two signals measured by W1 and W4 was used to determine whether the frequency deduced from the signals from W2 and W3 adequately represents those of a coherent structure. When the maximum cross-correlation coefficient of the W1 and W4 signals was greater than 0.8, the frequency found from the autoregressive (AR) spectrum was regarded as the vortex-shedding frequency. The vertical traverse of W3 was restricted from $y/c = -0.16$ to 0.21. The probe traversed was made with increments of 0.25 mm for $|y/c| \leqslant 0.05$ and, outside of this range, the measurement was carried out with a 0.5 mm interval.

3.2. Data reduction

A typical velocity signal in the wake of an oscillating airfoil can be decomposed into four components: the mean (time-averaged) velocity component, the velocity component induced by the airfoil motion, the large-scale velocity component generated by the vortex-shedding, and the random component. Since the frequency of the airfoil motion is known, we can single out the corresponding component from the measured signal using the phase-averaging technique. By phase-averaging the raw signal (Fig. 2(a)), the airfoil-induced component can be estimated as shown in Fig. 2(b). The sum of the large-scale component due to vortex-shedding and the random component can be obtained by subtracting the time-mean and the phase-averaged airfoil-induced component from the original signal, as shown in Fig. 2(c), which is used for the frequency analysis of vortex-shedding component.

For the spectral analysis of the vortex-shedding component, which is expected to vary with the instantaneous angle of attack, we need to adopt a method that can deal with frequency and time simultaneously. Since the AR spectrum has

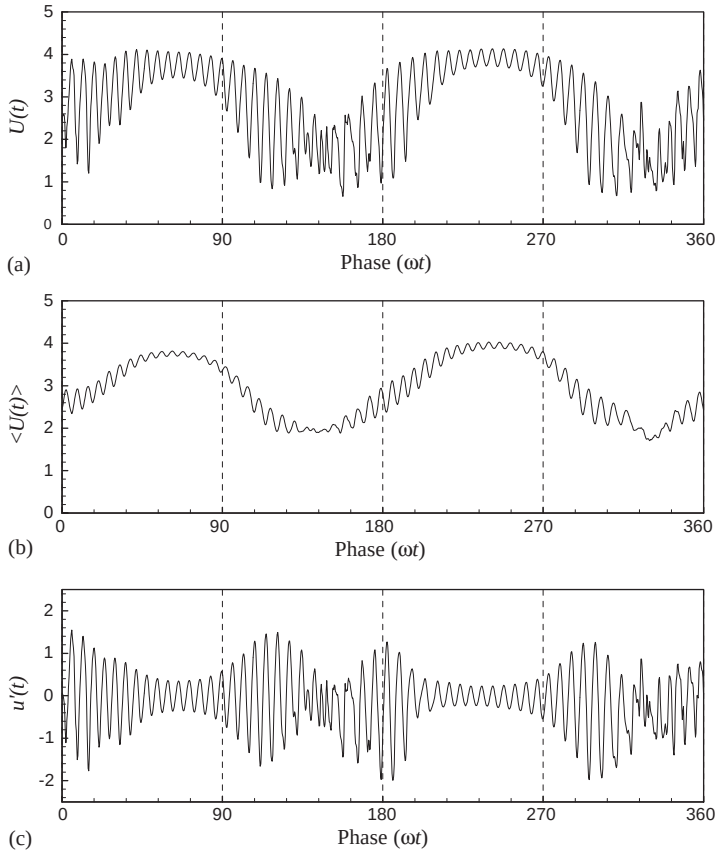

Fig. 2. Signal decomposition using phase-average technique: (a) original signal, (b) airfoil-induced signal, (c) vortex and random signal.

Table 1
Condition for the shedding frequency analysis using the AR method

Reduced frequency κ	Circular frequency ω	Sampling frequency f_s (kHz)	Window size, N	Δ phase angle (deg)
0.1	8	3	150	22.9
0.2	16	10	250	22.9
0.3	24	10	160	22.0
0.4	32	10	130	23.8

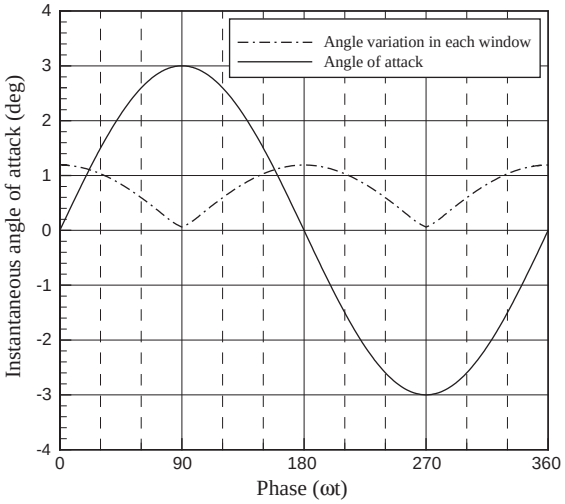

Fig. 3. Variation of angle of attack in each window.

higher resolution for short data records, the AR spectrum and the moving window were used to identify the time-varying vortex-shedding frequency. The methodology and condition for composing the short-time AR spectrum employed in the present study is similar to that reported by Jung and Park (2001). We changed the window size for each case as given in Table 1. Since the lowest shedding frequency of the present experiment is about 130 Hz, the window of 250 samples for the case of $\kappa = 0.2$ with 10 kHz sampling rate includes at least three cycles of vortex-shedding and the window of 130 samples for the case of $\kappa = 0.4$ includes about 1.7 cycles of the shedding. Using the AR method, Kamata and Ngamsritragul (1996) successfully performed the spectral analysis of the data that covers only 0.4 times the periodic cycle in their numerical experiment. Using the data over only 1.4 times the cycle, Jung and Park (2001) analyzed the unsteady frequency of the signal whose signal-to-noise ratio was −6 dB. Thus, we believe that the signal covering 1.7 cycles of a periodic record is sufficient to estimate the frequency with a high confidence level.

As the airfoil oscillates, the instantaneous angle of attack varies during the sampling. Also, the range of the angle of attack corresponding to one moving window varies with the reduced frequency. As shown in Table 1, the phase angle varies about 23° during the sampling of each window. Since the instantaneous angle of attack α is expressed as $\alpha = \alpha_1 \operatorname{Sin} \omega t$, the variation of the angle of attack in each window varies with the phase angle, as shown in Fig. 3. The minimum variation of the angle of attack is 0.06° when the phase angle of the window center is 90° and 270°, whereas the maximum variation is 1.17° when the phase angle of the window center is 0° and 180°. We assumed that the instantaneous angle of attack of the estimated spectrum from windowed data was equal to the angle of attack corresponding to the midpoint data of each window in the presentation of the results.

4. Results and discussion

4.1. Case of steady airfoil

For comparison purposes and as a preliminary work, measurements have been made of the wake for the case of steady airfoil at several angles of attack at the chord Reynolds number of 27 000. A typical vortex formation pattern is shown in Fig. 4(a), which can be represented by the double row of vortices. Fig. 4(b) illustrates a streamwise (U) and transverse (V) velocity signal detected at $x/c = 0.3$ and $y/c = 0$. In accord with Figs. 4(a) and (b), the U-velocity signal is doubly periodic when compared with the V-velocity signal. Thus, the frequency of the maximum peak of the spectrum of U-velocity, S_{uu}, is about two times the peak frequency of the V-velocity spectrum, S_{vv}, as shown in Fig. 4(c). This demonstrates that the shedding frequency is better found from the V-velocity signal, and hence the V-velocity signal was used throughout for frequency estimates in the present study.

For the steady airfoil, it is well known that at a constant Reynolds number the onset location of separation moves upstream while the boundary layer thickness at the trailing edge increases, and that the shedding frequency decreases

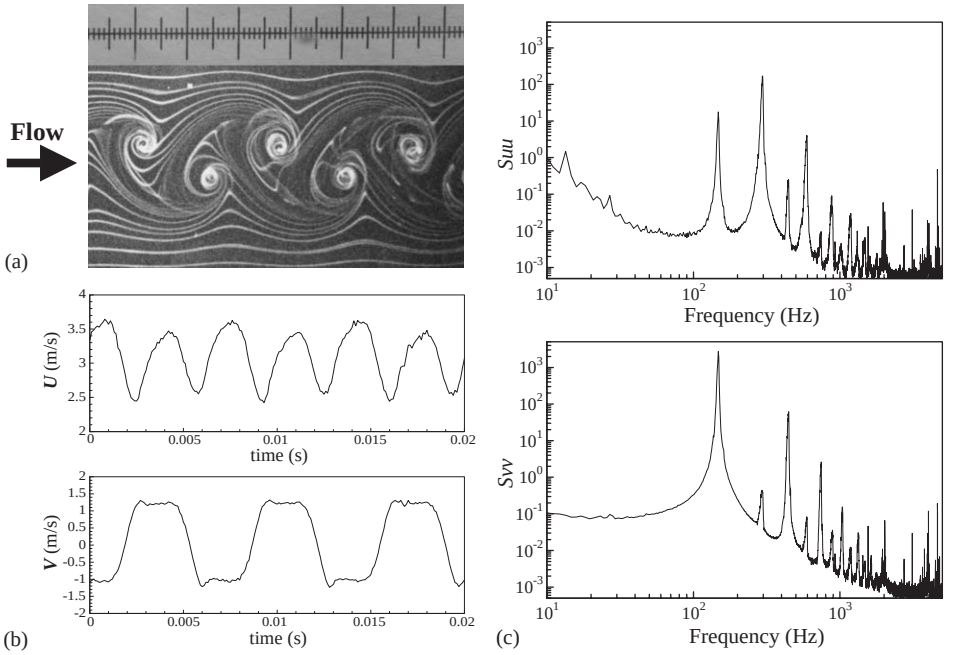

Fig. 4. (a) Visualization photograph; (b) signal measured at $x/c = 0.3$, $y/c = 0.0$, $\alpha = 0$; (c) spectra of streamwise and transverse velocity component.

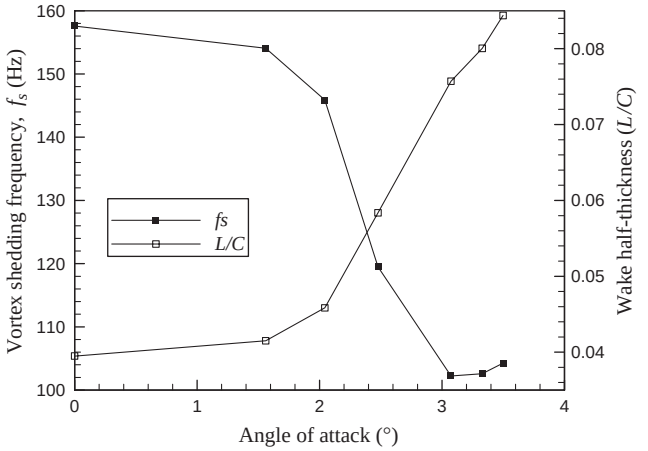

Fig. 5. Variation of vortex-shedding frequency and wake half-thickness of a steady airfoil with angle of attack at $x/c = 0.1$.

with an increase of angle of attack. To properly estimate the shedding frequency from the wake velocity measurement, we investigated the frequency variation with downstream distance from the trailing edge at zero angle of attack. The sampling frequency was 10 kHz. The vortex-shedding frequency was estimated by the FFT method and the signal of each segment consisted of 8192 samples. The ensemble-averaged spectrum of 6 estimates showed one sharp peak. From the transverse velocity signals measured from $x/c = 0.03$ to 1.0, the shedding frequency was found to be 153.6 ± 1.4 Hz with 95% confidence interval. Also, the shedding frequency variations with transverse distance between $y/c = -0.5$ and 0.5 at two downstream stations, $x/c = 0.1$ and 1.0 were checked out. The shedding frequency was estimated to be 153.9 ± 0.7 Hz at $x/c = 0.1$ and 153.9 ± 0.9 Hz at $x/c = 1.0$. The station $x/c = 0.1$ was in a wavy region where the streaklines are sinusoidal lines, and the station $x/c = 1.0$ was in a region where discrete vortices are clearly discernible in the streakline visualization (Jung, 2002). From these observations we concluded that the shedding frequency could be

estimated from the signals obtained anywhere in the x/c, y/c range mentioned above and, in terms of the Strouhal number based on airfoil thickness, was about 0.46. In a similar experiment to the present one, Bauer (1961) and Huang and Lin (1995) reported a Strouhal number of 0.43 and 0.47, respectively. From the wake centerline velocity curves with downstream distance, we found, after Owen and Johnson (1980), that the vortex formation region was up to $x/c<0.35$, and the region of roll-up completion started from $x/c = 0.45$. Thus, the shedding frequency can be estimated correctly either in the vortex formation region or in the roll-up completion region in the near wake.

The shedding frequency and the wake thickness variation with angle of attack are illustrated in Fig. 5. For the frequency estimation, we used the transverse velocity signal detected at $x/c = 0.1$ and $y/c = -0.05$, since the signal obtained at the pressure side of an airfoil was less contaminated by the random fluctuations than that at the suction side. If the angle of attack was larger than about $\alpha = 4^\circ$, the estimated spectrum was similar to a typical turbulence spectrum and there appeared no discernible frequency peak. The vortex-shedding in the wake is closely related to the boundary layer behavior on the airfoil surface. Because the variation of the boundary layer thickness can be deduced by the wake thickness, we also examined the wake half-thickness variation with the angle of attack. The present wake half-thickness was obtained by adding the half-thickness, at which the streamwise velocity becomes half of the free-stream velocity, of the upper surface wake (relative to the trailing edge) and that of the lower surface wake at $x/c = 0.1$. As illustrated in Fig. 5, the vortex-shedding frequency decreased from 157 to 102 Hz as the angle of attack increased from 0° to 3°. It is noted that the region of sharp decrease of the shedding frequency coincides with the region of the rapid increase of the wake thickness.

4.2. Case of oscillating airfoil

Fig. 6 shows the chronological flow patterns around the airfoil for $\kappa = 0.2$ at several instantaneous angles of attack. As shown in Fig. 6, the wake vortex patterns exemplify Karman vortex-shedding. We comment here that

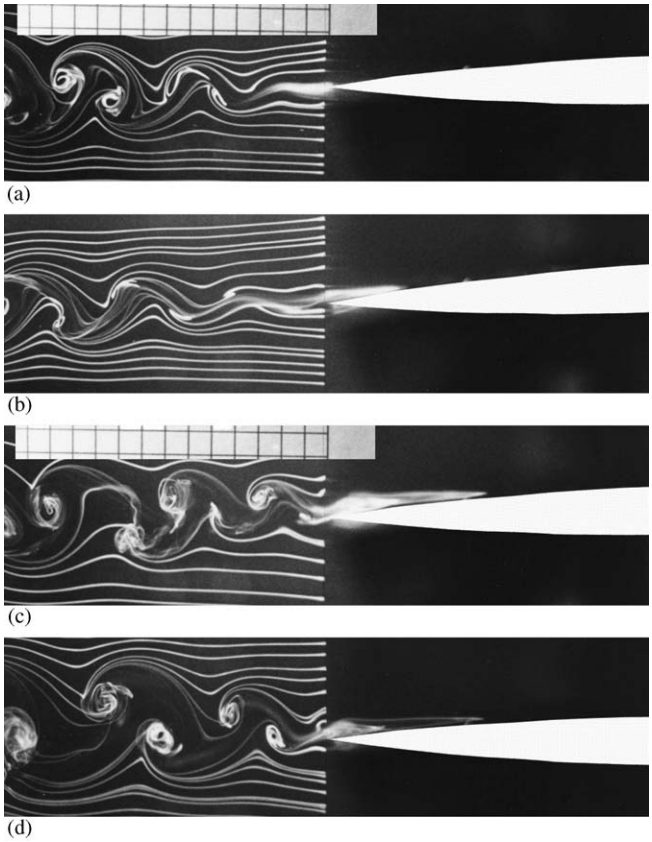

Fig. 6. Chronological flow patterns ($\kappa = 0.2$): (a) $\alpha = 1.5^\circ$, $\omega t = 30^\circ$; (b) $\alpha = 3^\circ$, $\omega t = 90^\circ$; (c) $\alpha = 1.5$, $\omega t = 150^\circ$; (d) $\alpha = 0^\circ$, $\omega t = 180^\circ$. The direction of the flow is from right to left. (one block of the ruler is 0.5 cm; (a) in pitch-up, (c) in pitch-down stroke).

the wake pattern at 3° angle of attack for the case of steady airfoil was intermittent or turbulent (Jung, 2002). As clearly seen from the plates of Figs. 6 and 7, all the flow patterns in the oscillating airfoil case are far from being turbulent. It is also noticed that the thin layer of reverse flow on the airfoil surface in pitch-down stroke (Fig. 6(c)) extends further upstream than in pitch-up stroke (Fig. 6(b)), regardless of the instantaneous angle of attack. In contrast to the steady flow, this signifies that the wake thickness varies strongly with the phase angle rather than with the angle of attack. This demonstrates that the boundary layer and the wake development of an oscillating airfoil are very much different from those of a steady airfoil. Kim and Park (1988) discussed in detail the reverse flow behavior and unsteady boundary layer separation in an oscillating airfoil at low Reynolds number.

The flow patterns around the airfoil at several instantaneous angles of attack for the case of $\kappa = 0.4$ are given in Fig. 7. Comparison of Fig. 7 with Fig. 6 convinces us that the degree of change in the wake pattern and the boundary layer flow with the instantaneous angle of attack becomes less when κ is larger. In fact, the wake patterns of Fig. 7 suggest that the boundary layer on the oscillating airfoil at $\kappa = 0.4$ remains laminar during the whole cycle of oscillation. Lee and Basu (1998) found that the oscillatory motion of the airfoil made the boundary layer remain attached for a much wider range of angle of attack when compared to the case of steady airfoil.

Figs. 8 and 9 contain, respectively, the mean velocity and the r.m.s. transverse velocity profiles for four reduced frequencies. These figures illustrate that the wake thickness variation becomes smaller and the wake becomes less turbulent as the reduced frequency increases, as reported in Park et al. (1990). It is noted that the r.m.s. velocity profiles for $\kappa = 0.1$ and 0.2 are much different from those for $\kappa = 0.3$ and 0.4 in that the profiles of $\kappa = 0.3$ and 0.4 have well defined double peak structure at all phase angles while those of $\kappa = 0.1$ and 0.2 have much broader and high turbulence intensity regions without double peak structure at some regions of the phase angle.

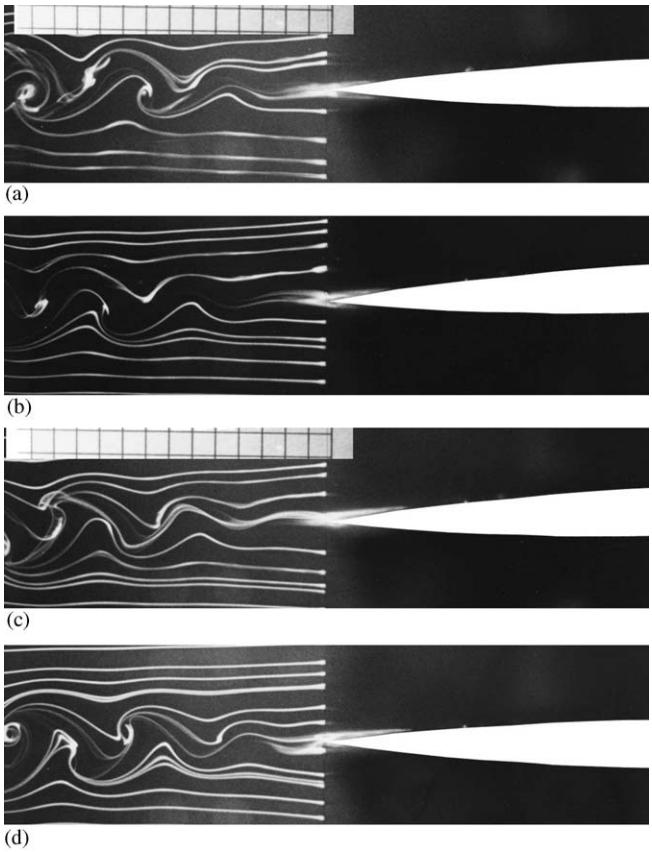

Fig. 7. Chronological flow patterns ($\kappa = 0.4$): (a) $\alpha = 1.5°$, $\omega t = 30°$; (b) $\alpha = 3°$, $\omega t = 90°$; (c) $\alpha = 2.1°$, $\omega t = 135°$; (d) $\alpha = 0°$, $\omega t = 180°$. The direction of the flow is from right to left.

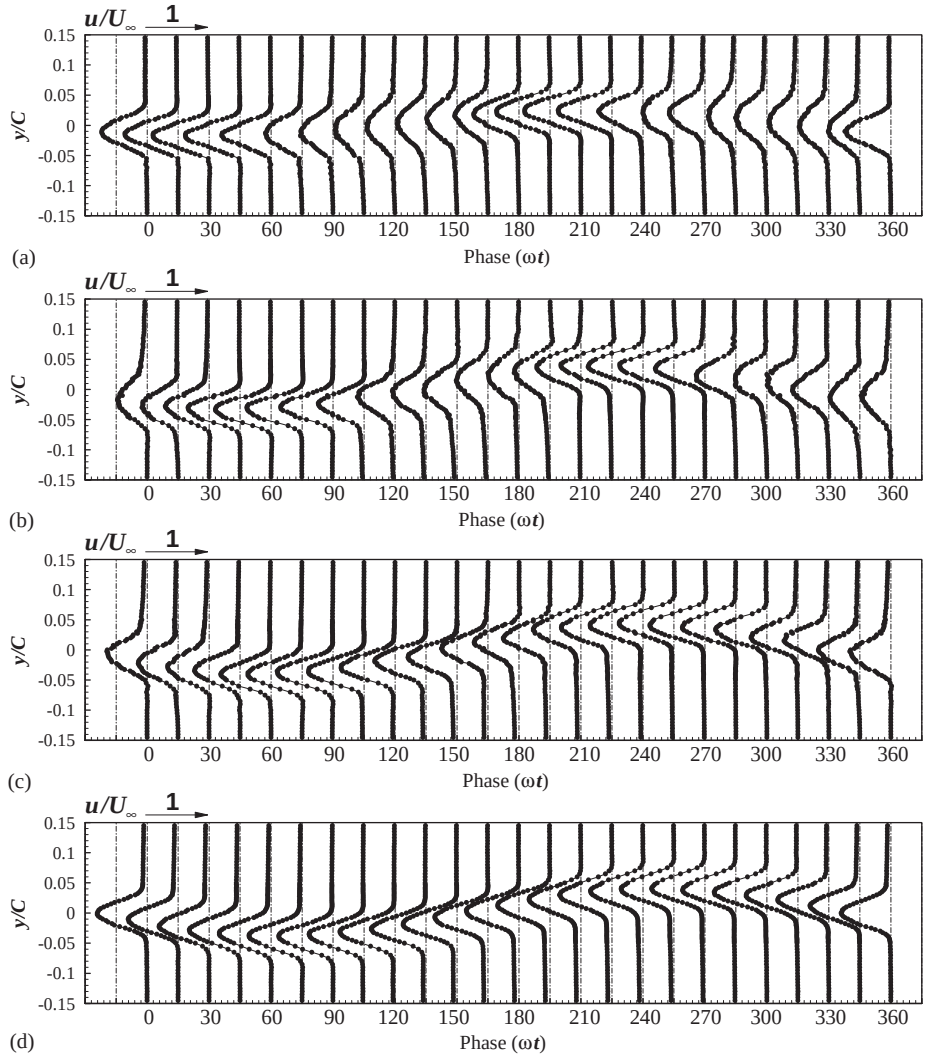

Fig. 8. Streamwise mean velocity profile ($x/c = 0.1$): (a) $\kappa = 0.1$, (b) $\kappa = 0.2$, (c) $\kappa = 0.3$, (d) $\kappa = 0.4$.

4.3. Frequency analysis

As mentioned earlier, the AR method and the moving window were used to estimate the vortex-shedding frequency. In the wake of an oscillating airfoil, there exists a phase-lag between the motion of the trailing edge and the signal measured at a downstream station (Park et al., 1990). To minimize the phase-lag, it was thus necessary to obtain the velocity signal at a location nearest to the trailing edge. However, if the measurement position were too close to the trailing edge, the signal would be contaminated by the reverse flow. Based on the results of flow visualization and the steady airfoil measurement (Section 4.1), we chose the measurement position to be at $x/c = 0.1$.

Fig. 10 shows the AR spectrum of each windowed data for the case of $\kappa = 0.2$. The upper part of this figure shows the windowed signal and the lower part shows the AR spectrum corresponding to the windowed data. Fig. 10 clearly illustrates that the AR spectrum provides us with a sharp peak to pinpoint the characteristic frequency. Fig. 11 displays the peak amplitude (of the AR spectrum) variations with the transverse coordinate associated with the shedding frequency. As can be expected, the peak amplitude profile generally resembles the r.m.s. velocity profile of Fig. 9(b). It is noted, however, that the peak amplitude profiles of Fig. 11 exhibit discontinuous features at several points. We conjecture that this is due to the inherent nature of the AR spectrum. While the power spectral density from the FFT method is proportional to the power of sinusoids present in the data, in an AR spectrum there is not often a linear

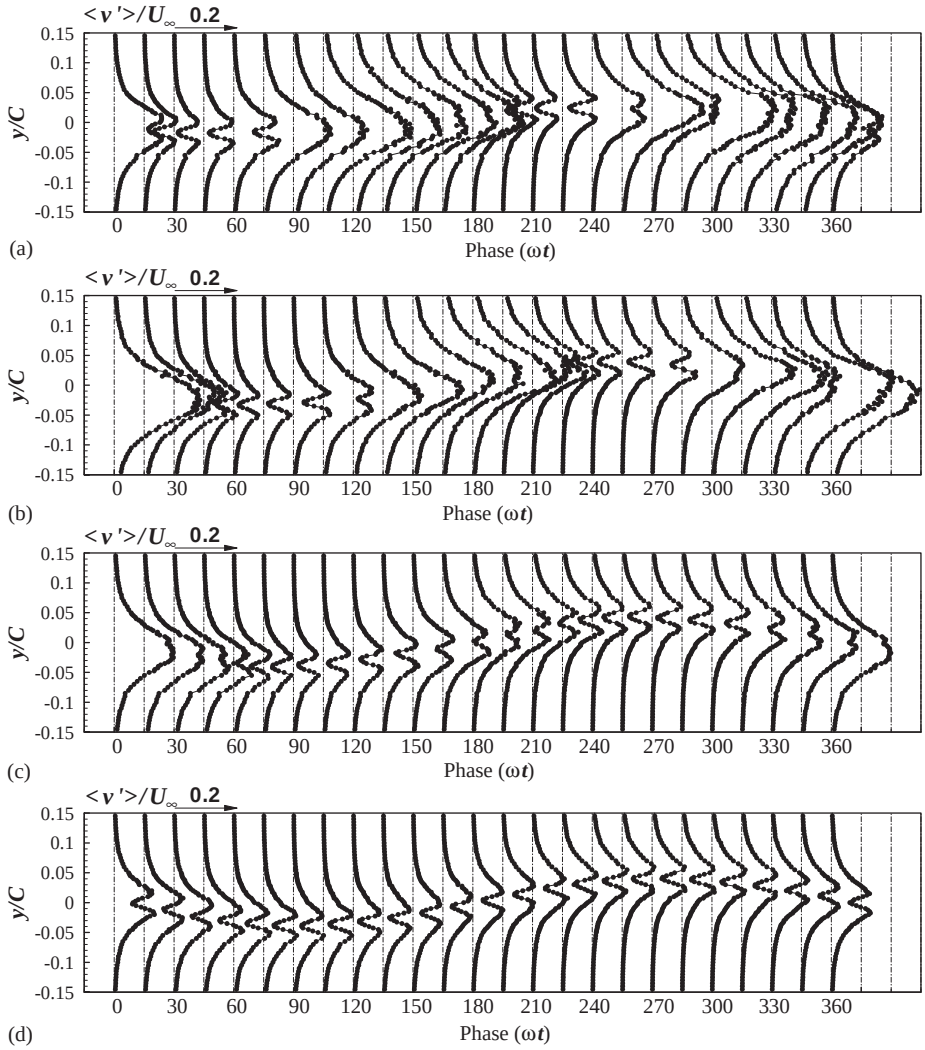

Fig. 9. Transverse r.m.s. velocity ($\sqrt{v'^2}/U_\infty$) profiles ($x/c = 0.1$): (a) $\kappa = 0.1$, (b) $\kappa = 0.2$, (c) $\kappa = 0.3$, (d) $\kappa = 0.4$.

relationship between the spectral peaks and sinusoidal power, since the amplitude and resolution of the AR spectrum is influenced by the signal-to-noise ratio.

Different from the case of the steady airfoil, the shedding frequency of the oscillating airfoil was found to vary with the transverse (y/c) location. This is illustrated in Fig. 12. When the airfoil oscillates with the amplitude of 3°, the trailing edge motion in vertical direction is confined in the range, $|y/c| \leqslant 0.039$. The velocity signal was measured at 33 stations from $y/c = -0.04$ to 0.04 at every 0.25 mm interval. The shedding frequency estimated from the data is given in Fig. 12. The gray scale indicates the frequency distribution. As shown in Fig. 12(a), when the reduced frequency is 0.2, the estimated shedding frequency is nearly independent of the measuring station; it varies only with the phase angle. However, as illustrated in Fig. 12(b), when the reduced frequency is 0.4, the shedding frequency varies with both the measuring station and the phase angle. It is seen that the shedding frequency variation follows the locus of the instantaneous trailing edge position. We thus picked up the shedding frequency determined from the transverse velocity signal measured at the nearest station to the trailing edge at every instant of oscillation.

Fig. 13 illustrates the variation of the shedding frequency at four reduced frequencies. In each plate, the vertical bar denotes the uncertainty of the frequency at each instantaneous angle of attack with a 95% confidence level. For the estimates of the frequency and the uncertainty analysis, 250 ensembles were used. Prior to the uncertainty analysis of the unsteady data, we first examined the uncertainty of the shedding frequency for the case of a steady airfoil. For the steady cases of $\alpha = 0°$ and 3°, the estimated frequencies from the FFT method were 157.5 and 102.1 Hz, respectively.

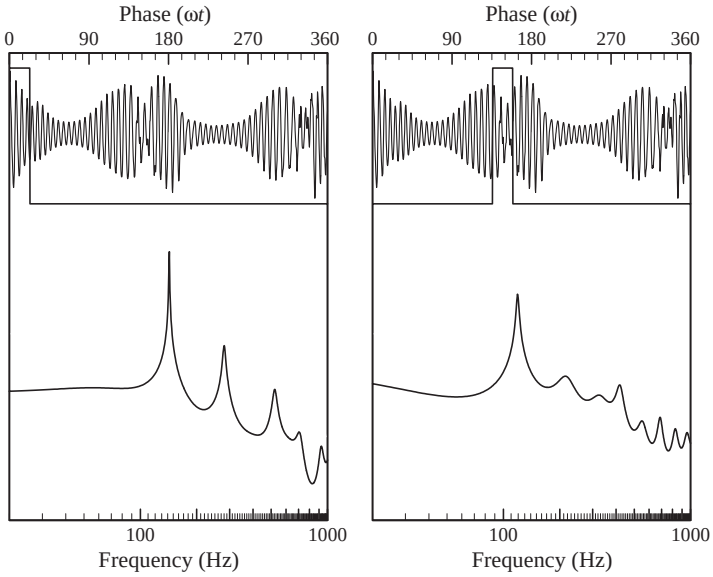

Fig. 10. AR spectrum for each segment ($\kappa = 0.2$).

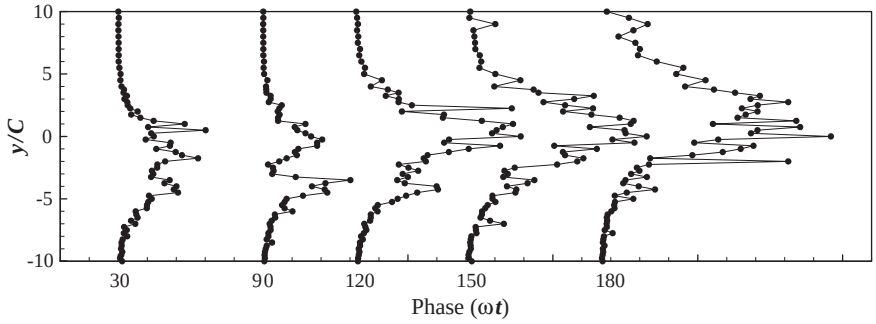

Fig. 11. Peak amplitude profiles associated to the shedding frequency ($x/c = 0.1$; $K = 0.2$).

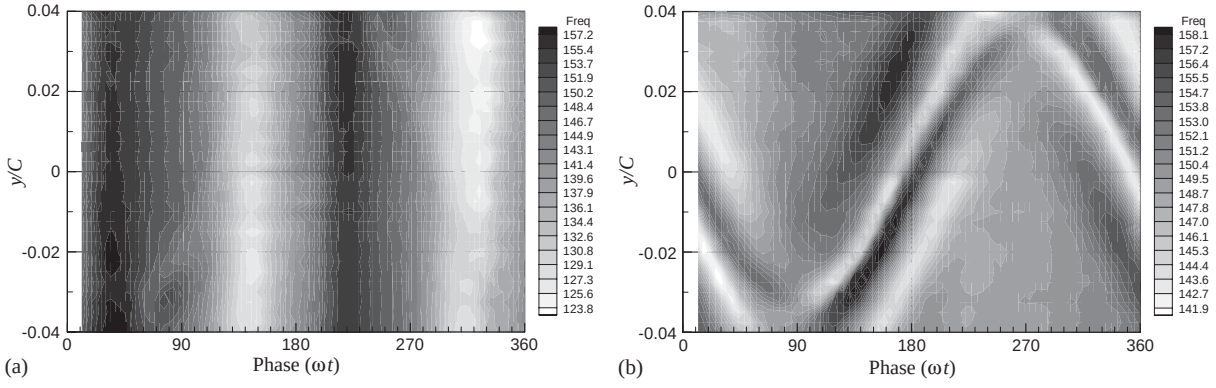

Fig. 12. Shedding frequency variation with transverse location at $x/c = 0.1$: (a) $\kappa = 0.2$, (b) $\kappa = 0.4$.

We evaluated the frequency of each segment with the data length of 250 samples by the AR method. Out of 200 estimates of each segment, the shedding frequency at a given angle of attack was determined. For the case $\alpha = 0^\circ$, we found that the peak frequencies identified by the AR method were within 157.4 ± 1.1 Hz with a 95% confidence level.

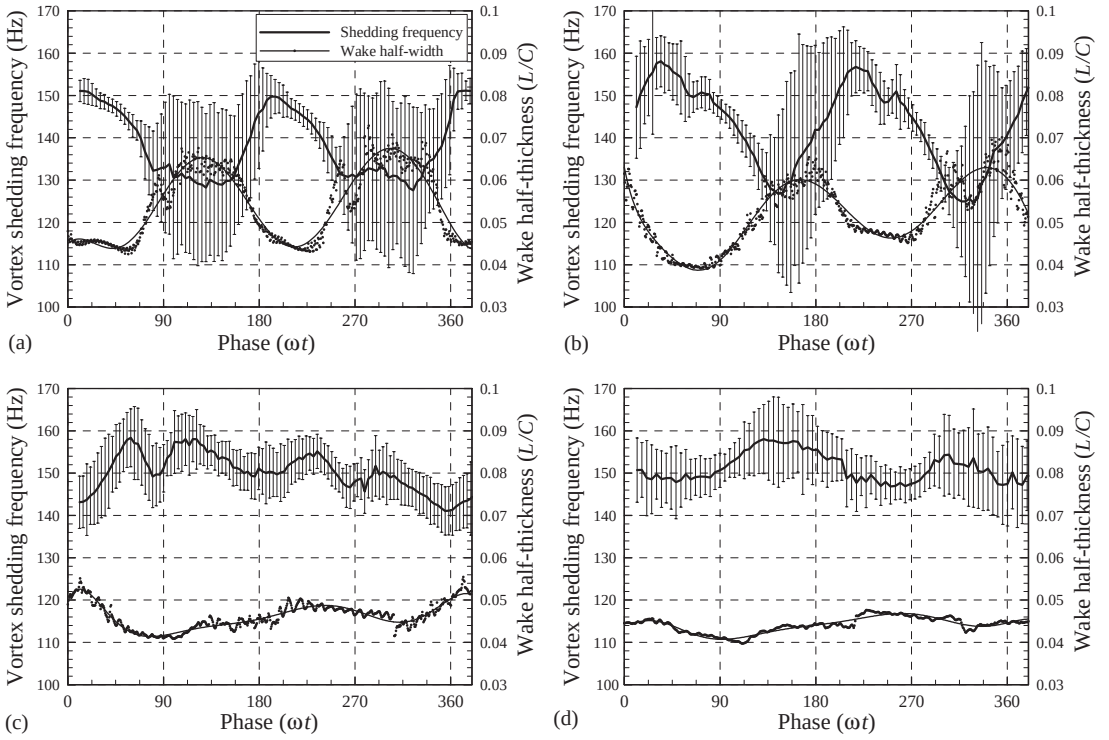

Fig. 13. Variation of the shedding frequency and the wake half-thickness: (a) $\kappa = 0.1$, (b) $\kappa = 0.2$, (c) $\kappa = 0.3$, (d) $\kappa = 0.4$.

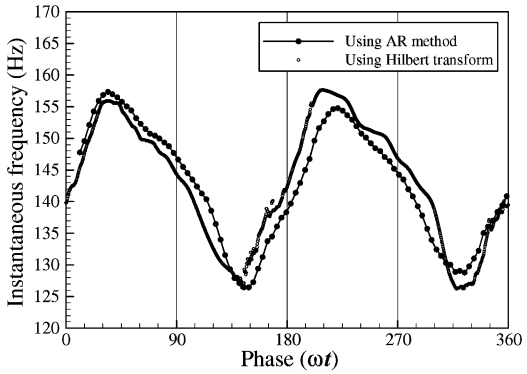

Fig. 14. Variation of the shedding frequency from the Hilbert transform ($\kappa = 0.2$).

For the case of $\alpha = 3^\circ$, the estimated peak frequencies were within 103.5 ± 18.1 Hz with a 95% confidence level. We find that the mean value so obtained was similar to the value from the FFT method. Since the wake flow at $\alpha = 3^\circ$ was more intermittent or turbulent, the uncertainty of the frequency was larger. For the case of $\kappa = 0.1$, the maximum uncertainty estimate was about equal to that of the steady airfoil at $\alpha = 3^\circ$. As the reduced frequency increases, the uncertainty of the estimated frequency decreases, as can be seen in Fig. 13. For the case of $\kappa = 0.2$ (Fig. 13(b)), the uncertainty is seen to increase when the phase angle is in the range $150^\circ \leqslant \omega t \leqslant 210^\circ$ where the airfoil is in pitch-down stroke. From the r.m.s. velocity profiles of Fig. 9(b), we see that the wake is rather broad and the r.m.s. fluctuations are much larger in this range signifying that the wake is more turbulent. The instantaneous shedding frequency can also be obtained by using the Hilbert transform (Bendat and Piersol, 1986). We applied the Hilbert transform to the signal for the case of $\kappa = 0.2$, the result of which is presented in Fig. 14. We find that the instantaneous shedding frequency obtained by using the Hilbert transform is in good agreement with that of the AR method. However, we should point out here that the

raw signal must be band-pass filtered between 80 and 180 Hz prior to the application of the Hilbert transform. If not, it was not possible to obtain a reasonable shedding frequency variation. In this sense, the AR method can be said to be more robust for the analysis of signals with non-negligible random fluctuations.

In Fig. 13, the variation of the wake half-thickness is also included. For the cases of $\kappa = 0.1$ (Fig. 13(a)) and $\kappa = 0.2$ (Fig. 13(b)), the wake half-thickness variation is nearly 90° out of phase to the frequency variation. For the cases of $\kappa = 0.3$ (Fig. 13(c)) and $\kappa = 0.4$ (Fig. 13(d)), both the variation of the wake half-thickness and the variation of the shedding frequency behave similarly. The variations of the wake thickness and of the shedding frequency with the phase angle are considerably smaller for the cases of $\kappa = 0.3$ and 0.4. For steady airfoil, it is known that the Karman vortex-shedding frequency decreases with the increase of an angle of attack [see Fig. 5 and Huang and Lin (1995)]. However, for an oscillating airfoil, these tendencies no longer hold. For the case of $\kappa = 0.2$ (Fig. 13(b)), even if the instantaneous angle of attack decreases from the maximum angle of attack, the shedding frequency continues to decrease. In this case, the shedding frequency is found to vary from 130 to 160 Hz, whereas the shedding frequency of a steady airfoil varied from 157 and 102 Hz as the angle of attack was changed from 0° to 3°. Fig. 13 indicates a trend that the variation of the shedding frequency with the phase angle becomes smaller when the reduced frequency is larger. Further, the amount of the shedding frequency variation is significantly reduced by the oscillation. The reduction is due to the behavior of the boundary layer. The oscillatory motion of the airfoil makes the boundary layer remain attached for a much wider range angle of attack compared with the steady airfoil. The radical difference in the shedding frequency variations of Figs. 13(a) and (b) and those of Figs. 13(c) and (d) can be attributed to the wake behavior demonstrated in Fig. 9. From Fig. 9, we confirm that the near-wake for $\kappa = 0.1$ and 0.2 behaves similarly, including the broad and high-intensity turbulence regions during a cycle of oscillation, in contrast to those for the cases of $\kappa = 0.3$ and 0.4. The wakes for $\kappa = 0.1$ and 0.2 are obviously more turbulent than those for $\kappa = 0.3$ and 0.4 as the profiles indicate.

5. Conclusions

We investigated the frequency characteristics of Karman vortex shedding in the near-wake of an oscillating airfoil through hot-wire measurements and a smoke-wire flow visualization. For the shedding frequency estimation of an oscillating airfoil, we used the autoregressive (AR) method and the moving window technique.

For the case of a steady airfoil, the shedding frequency decreases with increasing angle of attack. This tendency no longer holds for the case of an oscillating airfoil. For example, for the case of $\kappa = 0.2$, even if the instantaneous angle of attack decreased from the maximum angle of attack, the shedding frequency continued to decrease and the minimum shedding frequency was obtained at $\alpha = 18°$ and $\omega t = 145°$ (pitch-down stroke).

The range of the shedding frequency variation became smaller for the case of an oscillating airfoil than that for a steady airfoil. It was further found that the frequency variation during the cycle of oscillation diminished as the reduced frequency of oscillation increased.

Acknowledgements

This work was supported in part by the Korea Science and Engineering Foundation through grant number R01-1999-000-00264-0 and the Brain Korea 21 project at KAIST. Constructive suggestions offered by the anonymous reviewers to improve the quality of the paper are also gratefully acknowledged.

References

Bauer, A.B., 1961. Vortex-shedding from thin flat plates parallel to the free stream. Journal of the Aerospace Sciences 28, 340–341.

Bendat, J.S., Piersol, A.G., 1986. Random Data, second ed. Wiley-Interscience, New York (Chapter 13).

Carr, L.W., McAlister, K.W., McCroskey, W. J., 1977. Analysis of the development of dynamic stall based on oscillating airfoil experiments. NASA TN D-8382.

Chang, J.W., Eun, H., 2003. Reduced frequency effects on the near-wake of an oscillating elliptic wing. KSME International Journal 17, 1234–1245.

Hsiao, F.B., Liu, C.F., Tang, Z., 1989. Aerodynamic performance and flow structure studies of a low Reynolds number airfoil. AIAA Journal 27, 129–137.

Huang, R.F., Lin, C.L., 1995. Vortex-shedding and shear-layer instability of wing at low-Reynolds numbers. AIAA Journal 33, 1398–1403.

Jung, Y.W., 2002, Vortex-shedding in the near wake of an oscillating airfoil. Ph.D. Thesis, Division of Aerospace Engineering, KAIST (in Korean).

Jung, Y.W., Park, S.O., 2001. Application of the autoregressive method to the spectral analysis of a flow signal. Experiments in Fluids 31, 608–614.

Kamata, M., Ngamsritragul, P., 1996. Spectrum analysis by autoregressive methods (Performance on application to stationary signals). JSME International Journal, Series C 39, 179–187.

Kay, S., 1982. Modern Spectral Estimation: Theory and Application. Prentice-Hall, Englewood Cliffs, NJ.

Kim, J.S., Park, S.O., 1988. Smoke wire visualization of unsteady separation over an oscillating airfoil. AIAA Journal 26, 1408–1410.

Koochesfahani, M.M., 1989. Vortical pattern in the wake of an oscillating airfoil. AIAA Journal 27, 1200–1205.

Lee, T., Basu, T., 1998. Measurement of unsteady boundary layer developed on an oscillating airfoil using multiple hot-film sensors. Experiments in Fluids 25, 108–117.

Lissaman, P.B.S., 1983. Low-Reynolds-number airfoils. Annual Review of Fluid Mechanics 15, 223–239.

Marple, S.L., 1987. Digital Spectral Analysis with Applications. Prentice-Hall, Englewood Cliffs.

Owen, F.K., Johnson, D.A., 1980. Measurements of unsteady vortex flowfields. AIAA Journal 18, 1173–1179.

Park, S.O., Kim, J.S., Lee, B.I., 1990. Hot-wire measurements of near wakes behind an oscillating airfoil. AIAA Journal 28, 22–28.

Stuber, K., Gharib, M., 1990. Transition from order to chaos in the wake of an airfoil. Journal of Fluid Mechanics 213, 29–57.

Triantafyllou, M.S., Triantafyllou, G.S., Gopalkrishnan, R., 1991. Wake mechanics for thrust generation in oscillating foils. Physics of Fluids 3, 2835–2837.